DOI: 10.1002/ejic.201100179

2-(1-Acetyl-2-oxopropyl)-5,10,15,20-tetraphenylporphyrin and Its Transition-Metal Complexes

Hongshan He,*[a] Mukul Dubey,[a] Yihan Zhong,[a] Maheshwar Shrestha,[a] and Andrew G. Sykes[b]

Keywords: Porphyrinoids / Dyes / Sensitizers / Solar cells / Nanotubes / Transition metals

The 2-(1-acetyl-2-oxopropyl)-5,10,15,20-tetraphenylporphyrin free base (H_2TPP-AOP) and its transition-metal complexes (MTPP-AOP, M = Cu^{2+}, Zn^{2+}) have been synthesized. Single-crystal X-ray diffraction analysis revealed that the 1-acetyl-2-oxopropyl (AOP) group is attached to a β-pyrrolic position through the methylene group. The mean plane of the AOP is almost perpendicular to the porphyrin ring. The zinc(II) complex crystallizes as a five-coordinate species with one methanol/water solvate in the axial position, whereas the copper(II) complex is four-coordinate. These compounds exhibit strong absorption in the UV and visible regions. The fluorescence lifetimes are 1.85 and 8.0 ns for the free base and zinc(II) complex, respectively. Density functional calculations indicate that these porphyrins are energetically suitable for electron injection from their lowest-unoccupied molecular orbitals to the conduction band of the titanium dioxide semiconductor. However, the energy conversion efficiencies of the three porphyrin-sensitized solar cells are low, that is, 0.14, 0.015 and 0.021 % for ZnTPP-AOP, CuTPP-AOP and H_2TPP-AOP, respectively. The poor photovoltaic performance is ascribed to the low dye-loading of these porphyrins on the titanium dioxide surface. The neighbouring phenyl groups exert sufficient steric hindrance on the AOP to limit its binding to the TiO_2 semiconductor.

Introduction

Dye-sensitized solar cells (DSCs) have been recognized as a key technology for the conversion of solar energy into electricity.[1] These devices are lightweight and can be adapted for a variety of indoor and outdoor applications, for example, as power supplies for cell phones, music players, laptops and toys.[2] The colourful appearance of DSCs also makes devices very attractive for installation on windows, walls and ceilings as decorations. However, there is no mass-produced commercial product available for technical reasons. For example, they have a low efficiency for the conversion of solar energy into electricity. As the overall energy conversion efficiency of a DSC is the product of light-harvesting efficiency (LHE), electron injection efficiency (η_{inj}) and electron collection efficiency (η_{coll}), high efficiencies can only be achieved by systematic engineering of dye molecules, interfaces between dye molecules, semiconductors and redox couples. DSCs with dye molecules with broader absorption ability and TiO_2 nanostructures with reduced electron recombination will lead to high efficiency. In state-of-the-art DSC devices, ruthenium(II) dyes with an optical onset at 750 nm and TiO_2 nanoparticles with diameters of about 20 nm are used, which have only around 11.6% efficiency in a single cell.[1] The efficiency from a module is much lower than this, usually between 4 and 8%.[2] Thus, new light-harvesting materials and nanoscale semiconductors are needed to advance this technology.

Porphyrins are one type of dye that show promise for cost-effective DSCs. Porphyrins usually exhibit strong absorption in the UV and visible regions with high absorption coefficients. They are easy to make and modify and are ideal candidates for lightweight devices. Numerous porphyrin dyes have been synthesized and their photovoltaic performances have been tested. However, significant achievements have only been made recently.[3–17] For example, Campbell et al.[16] linked a penta-2,4-dienoic acid group to the β-pyrrolic position of a zinc porphyrin and an energy conversion efficiency of 7.1% was achieved as a result of efficient electronic coupling of the porphyrin to TiO_2 through a conjugated linker. Imahori and co-workers[4,6,11,18,19] found that bulky mesityl groups can reduce aggregation. When one diarylamino group was introduced at a *meso* position of a porphyrin with 4-benzoic acid as an anchoring group, the cell exhibited an efficiency of 6.5%. These authors also fused quinoxaline onto the β-pyrrolic ring and the resulting cells gave a maximum energy conversion efficiency of 5.2%. Liu et al.[10] conjugated a thiophene moiety to a *meso* position of porphyrin and 5.1% efficiency was obtained. Diau and co-workers[9,12,13,20] in-

[a] Center for Advanced Photovoltaics, South Dakota State University,
Brookings, SD 57007, USA
Fax: +1-605-688-4401
E-mail: hongshan.he@sdstate.edu
[b] Department of Chemistry, University of South Dakota, Vermillion, SD 56069, USA

Supporting information for this article is available on the WWW under http://dx.doi.org/10.1002/ejic.201100179.

vestigated phenylethynyl-substituted porphyrins systematically and found porphyrins with a donor–acceptor structure exhibited very good photovoltaic performance. When the cell was co-sensitized with another complementary indoline-based dye,[21] an energy conversion efficiency of around 10% was obtained. These results demonstrate the potential of porphyrin-based dyes for the development of cost-effective solar cells. We are very interested in porphyrin dyes and synthesized three 1-acetyl-2-oxopropyl (AOP)-functionalized porphyrins (see Scheme 1). It was hoped that the AOP group would act as an alternative to the carboxylic group (COOH) as binding group for efficient electron injection. However, the results show that the photovoltaic performance of these porphyrins is poor. It was found that steric hindrance around the anchoring group prevents binding of the AOP to the TiO_2 semiconductor. This leads to a very low dye-loading. Reported herein are the details of the synthesis of these porphyrins, their structures, photophysical properties and photovoltaic performance.

Results and Discussion

Snthesis and Structural Characterization

The 1-acetyl-2-oxopropyl (AOP)-functionalized porphyrinatocopper(II) complex was prepared by the reaction of 2-nitroporphyrinatocopper(II) and acetylacetone in the presence of anhydrous K_2CO_3. The free base was prepared by demetallation of the copper(II) complex with concentrated H_2SO_4 and the zinc(II) complex was obtained by the direct reaction of the free base and zinc acetate (Scheme 1). All the compounds were purified by silica gel column chromatography. Their compositions were confirmed by elemental analysis and mass spectroscopy. Characteristic vibrations of υ_{C-H} and $\upsilon_{C=O}$ from the AOP group were observed at 3051, 3021 and 1594 cm^{-1} for H_2TPP-AOP, 3051, 3018 and 1596 cm^{-1} for CuTPP-AOP and 2957, 2927 and 1594 cm^{-1} for ZnTPP-AOP. An additional peak at 3327 cm^{-1} from the N–H vibration was also observed for H_2TPP-AOP.

The structures of the three compounds were further ascertained by single-crystal X-ray diffraction analysis. ZnTPP-AOP crystallizes in the monoclinic space group *C*2/*c*. The Zn^{2+} lies in the mean plane of N1/N2/N3/N4. It is five-coordinated with the four N atoms of the porphyrin ring and with one O atom from methanol/water binding directly to the central metal ion (Figure 1). The coordination geometry of Zn^{2+} is distorted square-pyramidal. The AOP group is linked to the porphyrin ring through its terminal propyl carbon with all of its five C atoms (C1–C5) and two O atoms (O2 and O3) in one plane. The O2 and O3 are hydrogen-bonded. The mean plane of the AOP is almost parallel to the neighbouring phenyl group P4 and perpendicular to the mean plane of N1/N2/N3/N4 with a torsion angle of 88.36(8)°. The phenyl groups P1, P2 and P4 are also almost perpendicular to the porphyrin ring with torsion angles of 89.23(10), 84.80(16) and 86.59(9)°, respectively. The phenyl group P3 exhibits a torsion angle of 61.70(0.10)° to the mean plane of the porphyrin ring. Note that one phenyl ring (P2) is disordered. In addition, water and methanol molecules share the axial coordination position in a ratio of 0.36:0.64.

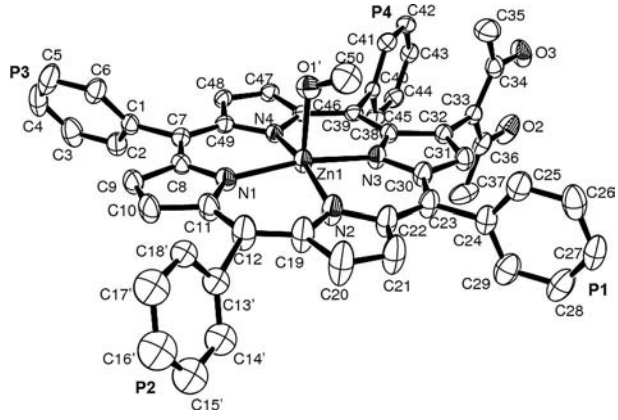

Figure 1. ORTEP diagram of ZnTPP-AOP·0.36CH_3OH·0.64H_2O with thermal ellipsoids drawn at the 50% probability level. The four phenyl groups are labelled as P1, P2, P3 and P4, respectively. Only O1′ of methanol is shown. The O1 of water was omitted for clarity. Selected bond lengths [Å]: N1–Zn1 = 2.071(3), N2–Zn1 = 2.043(3), N3–Zn1 = 2.086(2), N4–Zn1 = 2.049(2), O2–O3 = 2.4398(5), O1′–Zn1 = 2.082(11), O1–Zn1 = 2.31(2).

CuTPP-AOP crystallizes in the triclinic space group $P\bar{1}$. There are two molecules and two CH_2Cl_2 solvates in each asymmetric unit. The Cu^{2+} ion is coordinated by four N

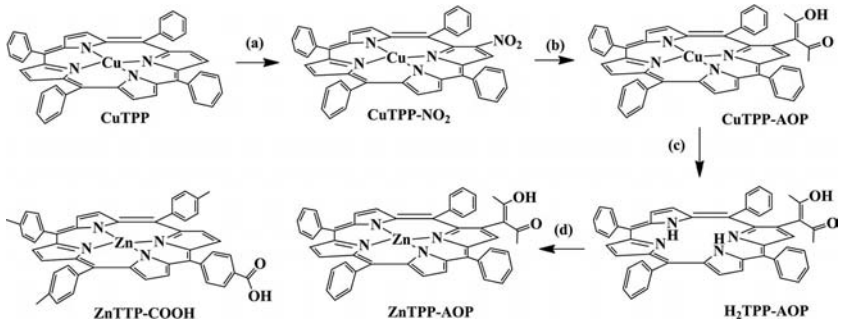

Scheme 1. Synthesis of 1-acetyl-2-oxopropyl (AOP)-functionalized porphyrins. The structure of a reference porphyrin ZnTTP-COOH is also shown. Reagents and conditions: (a) $Cu(NO_2)$, acetic anhydride, $CHCl_3$, RT, 24 h; (b) acetylacetone, DMSO, anhydrous K_2CO_3, 50 °C, 1 h; (c) H_2SO_4 (98%), CH_2Cl_2, 0.5 h, RT; (d) $Zn(OAc)_3$, MeOH/$CHCl_3$, RT, 12 h.

atoms from the porphyrin ring, as shown in Figure 2. The AOP group is also located at a β-pyrrolic position. Similar to the ZnTPP-AOP structure, the five C atoms (C1–C5) and two O atoms (O1 and O2) of the AOP group also lie in one plane with a torsion angle of 67.12(12)° to the mean plane of N1/N2/N3/N4. The torsion angles of the three phenyl groups P2, P3 and P4 with respect to the mean plane of N1/N2/N3/N4 are 50.81(17), 51.94(12) and 58.13(15)°, respectively. The only phenyl group that is almost perpendicular to the porphyrin ring is the P1 group, which has a torsion angle of 85.08(0.19)°. The H atom on O1 points away from O2, which indicates there is no hydrogen-bonding interaction between O1 and O2.

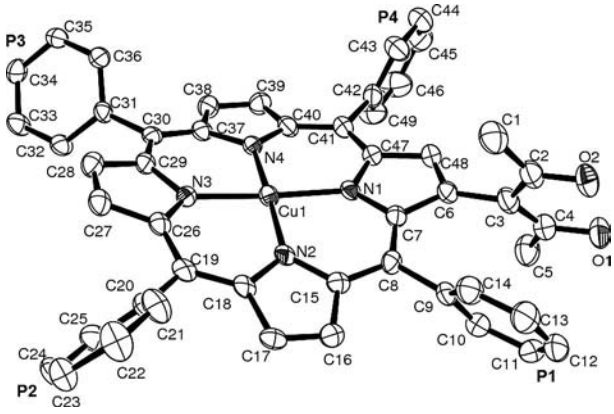

Figure 2. ORTEP diagram of CuTPP-AOP·CH_2Cl_2 with thermal ellipsoids drawn at the 50% probability level. The four phenyl groups are labelled as P1, P2, P3 and P4. The CH_2Cl_2 has been omitted for clarity. Selected bond lengths [Å]: N1–Cu1 2.000(4), N2–Cu1 1.973(4), N3–Cu1 1.992(4), N4–Cu1 1.984(4), O1–O2 2.468(6).

H_2TPP-AOP crystallizes in the monoclinic space group $P2_1/c$. The quality of the refined structure was poor. Attempts to grow high quality crystals were unsuccessful; however, it is quite clear from the refined structure that the AOP group is attached to the porphyrin ring. The structure is quite similar to those of ZnTPP-AOP and CuTPP-AOP (an ORTEP diagram of this structure is provided in Figure S1 of the Supporting Information).

The porphyrin moieties of the three compounds show different degrees of planarity. The side-views of the core structures of the three porphyrins are shown in Figure 3. The side-view of CuTPP, which has a perfect planar structure, is also presented as a reference.[22] In ZnTPP-AOP, the Zn^{2+} is 0.2400(17) Å above the porphyrin ring. The porphyrin ring is twisted to a small extent, which becomes more severe in H_2TPP-AOP. The CuTPP-AOP exhibits a saddled conformation with two pairs of pyrrole groups at opposite positions bending in opposite directions. The packing modes of the three porphyrins are also different (Figure S2). ZnTPP-AOP forms a chain structure as a result of an intermolecular hydrogen-bonding interaction between O1 and O3. CuTPP-AOP molecules are stacked one above another to form a layered structure. In H_2TPP-AOP, two sets of paired molecules align with each other at an angle of around 120° to form a zigzag structure.

Figure 3. Side-views of the porphyrin cores of (A) CuTPP-AOP, (B) ZnTPP-AOP, (C) H_2TPP-AOP and (D) CuTPP.

Photophysical Properties

The absorption spectra of the three porphyrins are very similar to each other. All compounds exhibit a strong absorption at around 420 nm (Soret band) and a weak absorption at 500–700 nm (Q bands; Figure 4). The spectra are very similar to those of their parent compounds, which indicates that the introduction of an AOP group at the β-pyrrolic position does not alter the absorption properties significantly. ZnTPP-AOP and H_2TPP-AOP exhibit typical fluorescence upon excitation (Figure S3). ZnTPP-AOP gives two emission peaks at 599 and 645 nm with a lifetime of 1.85 ns whereas H_2TPP-AOP exhibits two peaks at 655 and 718 nm with a lifetime of 8.0 ns. No fluorescence was observed for CuTPP-AOP. The quantum yields for ZnTPP-AOP and H_2TPP-AOP in ethanol are 4.5 and 2.8%, respectively. The fluorescence lifetimes are long enough for electron injection from the excited porphyrins to the conduction band of TiO_2 during the DSC operation, which usually occurs within a time-scale of <100 fs.[23]

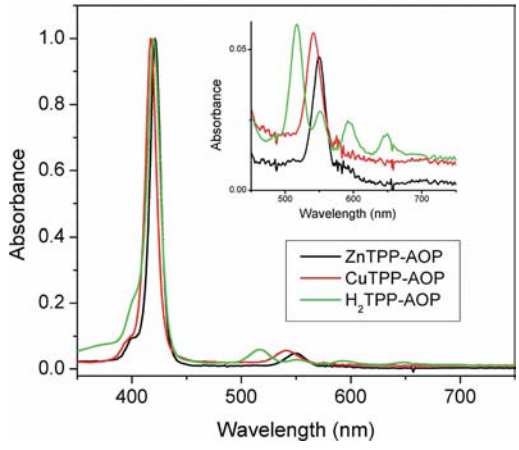

Figure 4. Normalized absorption spectra of three porphyrins in CH_2Cl_2 at room temperature.

Theoretical Calculations

As the HOMO (highest-occupied molecular orbital) and LUMO (lowest-unoccupied molecular orbital) energy levels of dyes are important for the normal operation of DSCs, density functional theory (DFT) studies were carried out to ensure the dyes are energetically suitable for electron injec-

tion. The calculated HOMO and LUMO energy levels of ZnTPP-AOP, CuTPP-AOP, H_2TPP-AOP and ZnTTP-COOH in acetonitrile along with the conduction and valence bands of TiO_2 nanoparticles are depicted in Figure 5. The LUMO energy levels of the three porphyrins are around –2.80 eV, which is higher than the conduction band of TiO_2 nanoparticles. This ensures electron injection from the porphyrin to the TiO_2 conduction band for the normal functioning of DSCs. However, the electron density distributions in these orbitals, as shown in Figure 6, are largely localized on the porphyrin ring. The electron density on the AOP group is relatively low. As electron delocalization on to the anchoring group usually facilitates electron injection and photovoltaic performance, the less delocalized molecular orbital on the AOP group may weaken their electron coupling to the TiO_2 conduction band. Note that delocalized orbitals are not the only means of electron injection, through-space injection is also possible.[4,11,14]

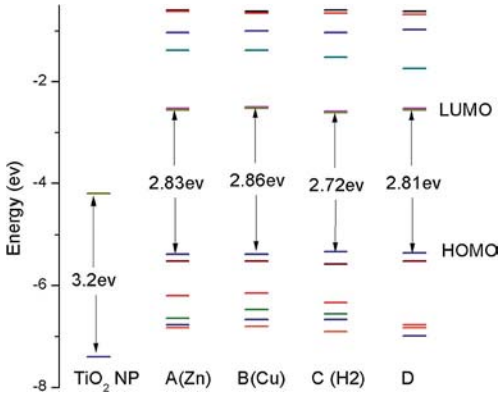

Figure 5. Calculated HOMO and LUMO energy levels of (A) ZnTPP-AOP, (B) CuTPP-AOP, (C) H_2TPP-AOP and (D) ZnTTP-COOH in acetonitrile from DFT calculations at the B3LYP/6-31G(D) level of theory.

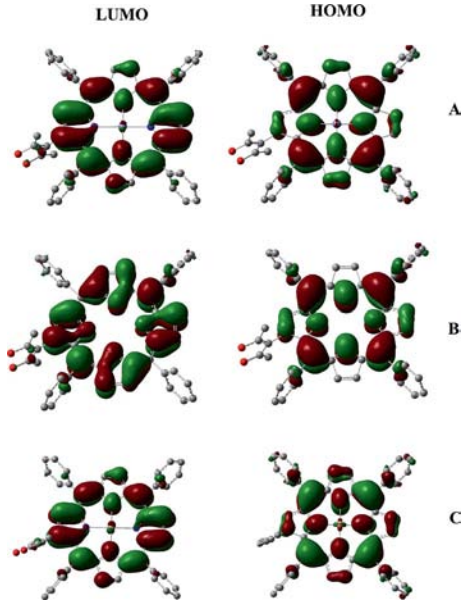

Figure 6. HOMO and LUMO profiles of (A) ZnTPP-AOP, (B) H_2TPP-AOP and (C) CuTPP-AOP in acetonitrile from DFT calculations at the B3LYP/6-31G(D) level of theory.

Photovoltaic Performance

The photovoltaic performances of the synthesized porphyrins were evaluated in titanium dioxide nanotube (TiO_2 NT) based DSCs. The TiO_2 NTs exhibit large specific surface areas, high pore volumes and excellent electron collection efficiency.[24–27] They were prepared by anodization of Ti foil under a constant DC voltage (60 V) in ethylene glycerol and detached in the presence of dilute HF, as reported previously.[28] Figure 7 shows the cross-sectional scanning electron microscopy (SEM) images of the TiO_2 NT film after sintering. The TiO_2 NTs are vertically aligned with lengths of around 20 μm. The diameters and wall thicknesses of the NTs are around 80 and 20 nm, respectively. After fixing the arrays on to the fluorine–tine–oxide (FTO) glass with the help of a thin layer of TiO_2 nanoparticles (≈3 μm), no clear morphological changes in the TiO_2 NTs were observed. The resulting film is opal. One side of the TiO_2 NTs are embedded inside the NP matrix and makes very good physical contact. The TiO_2 NT arrays are very easy to remove from the FTO glass if the TiO_2 NP layer is not applied. Note that the TiO_2 NTs are open at one end and closed at the other. The NTs with open ends facing the TiO_2 NP layer bind much more strongly to the FTO glass than the closed ends and are suitable for cell fabrication. Therefore only cells with this configuration were tested.

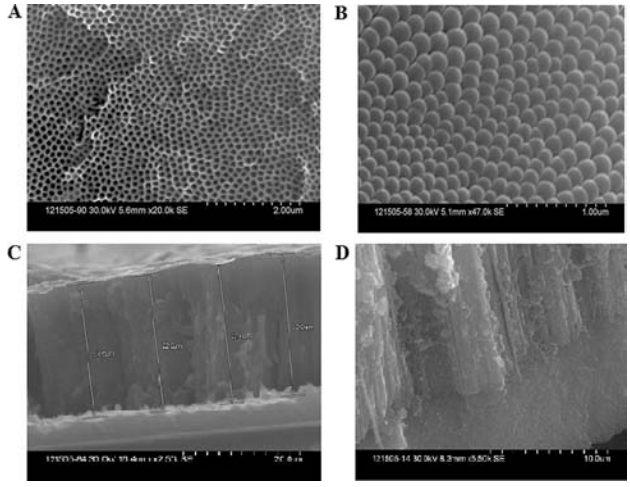

Figure 7. Scanning electron microscopy (SEM) images of (A) the open ends and (B) the closed ends of free-standing TiO_2 NT arrays. (C,D) Cross-sectional SEM images of TiO_2 NT arrays on FTO after sintering at 450 °C for 30 min in air. Image D is C with a higher magnification.

The photovoltaic performances of the three porphyrins were tested under AM1.5 conditions. The photovoltaic parameters are listed in Table 1. For comparison, the cell efficiencies of ZnTTP-COOH and a commercial ruthenium dye N719 under the same conditions are also listed in Table 1. Of the three synthesized porphyrins, ZnTPP-AOP gives the

highest energy conversion efficiency of 0.14%, whereas CuTPP-AOP and H_2TPP-AOP exhibit negligible energy conversion efficiency. Under the same conditions, ZnTTP-COOH and N719 show 2.43 and 6.1% energy conversion efficiency, respectively. Typical *J*–*V* curves for these cells are shown in Figure 8. The open-circuit voltages (V_{OC}), short-circuit current densities (J_{SC}) and fill factors (FF) of these cells are all lower than those of ZnTTP-COOH- and N719-sensitized cells. The IPCE (incident photon to current efficiency) profiles, as shown in Figure 9, are quite similar to the absorption spectra with high IPCE in the Soret band range and low IPCE in the Q-band range. The ZnTPP-AOP-sensitized cell exhibits 7% IPCE in the Soret band region, whereas the IPCE values of ZnTTP-COOH- and N719-sensitized cells are around 70 and 90% over a much wider spectral range.

Table 1. Photovoltaic parameters of DSCs with different porphyrins and N719 as dyes.

Dye	V_{OC} [mV]	J_{SC} [mA/cm^2]	FF [%]	η [%]
ZnTPP-AOP	530	0.41	65	0.14
CuTPP-AOP	480	0.06	53	0.015
H_2TPP-AOP	483	0.08	56	0.021
ZnTTP-COOH	612	5.70	70	2.43
N719	700	16.26	53	6.10

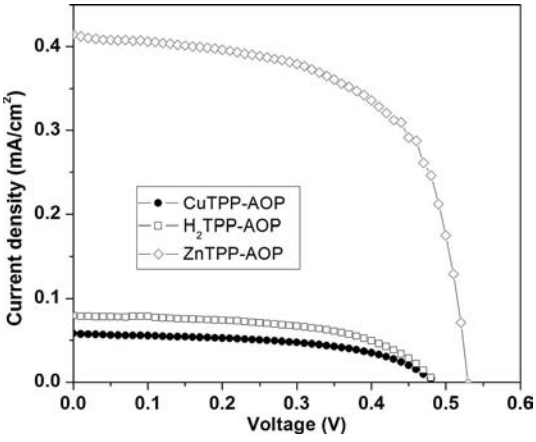

Figure 8. *J*–*V* curves of the ZnTPP-AOP-, CuTPP-AOP- and H_2TPP-AOP-sensitized DSCs.

The overall energy conversion efficiency of a DSC is the product of light-harvesting efficiency (LHE), electron injection efficiency (η_{inj}) and electron collection efficiency (η_{coll}). However, given their similar photophysical properties and the orthogonal arrangement of the anchoring group relative to ZnTTP-COOH, the poor photovoltaic performances of the three porphyrins can only be ascribed to their low dye-loading on the TiO_2 film. It was found that the TiO_2 films after porphyrin impregnation for 12 h were slightly yellow, whereas the films of ZnTTP-COOH were deep purple, as shown in the inset of Figure 9. The addition of pyridine did not improve the loading density. It is unlikely that the poor dye-loading is a result of the intrinsic binding ability of AOP to TiO_2. Instead, the steric hindrance of the phenyl group adjacent to the AOP plays a significant role. The single-crystal structure analysis reveals that the AOP group is close to the adjacent phenyl group and the AOP is too short to allow effective binding to the titanium atom; this situation does not occur with the longer ZnTTP-COOH, as shown schematically in Figure 10. In this regard, removing the adjacent phenyl group could enhance the binding of AOP to the TiO_2 surface. Currently we are working in this direction and results will be reported in due course.

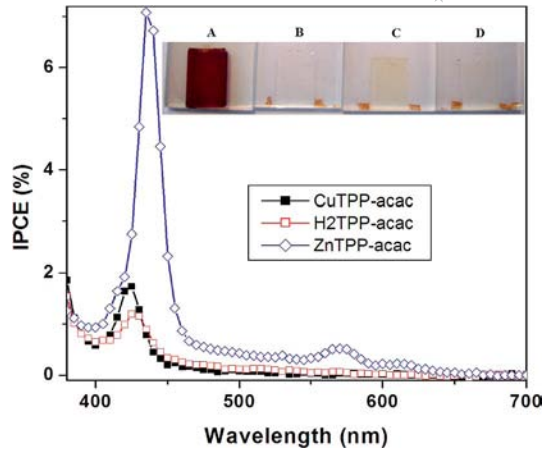

Figure 9. IPCE spectra of ZnTPP-AOP-, CuTPP-AOP- and H_2TPP-AOP-sensitized DSCs. The insets show the optical images of TiO_2 NT films coated with (A) ZnTTP-COOH, (B) H_2TPP-AOP, (C) ZnTPP-AOP and (D) CuTPP-AOP.

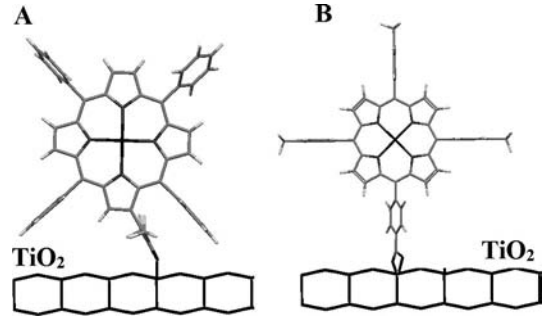

Figure 10. Possible alignments of (A) ZnTPP-AOP and (B) ZnTTP-COOH on the surface of TiO_2 nanotubes.

Conclusions

Three asymmetric porphyrins have been synthesized and their structures characterized by single-crystal X-ray diffraction analysis. The 1-acetyl-2-oxopropyl (AOP) group is linked to a β-pyrrolic position. The mean plane of the AOP is almost perpendicular to the mean plane of the porphyrin ring. Theoretical calculations and photophysical properties indicate that these porphyrins are suitable for the normal operation of DSCs. However, the neighbouring phenyl groups of the AOP prevent their binding to TiO_2 nanotubes. As a result, the photovoltaic performances of these porphyrins are quite poor. The zinc compound exhibits 0.14% energy conversion efficiency, whereas the reference dyes ZnTTP-COOH- and N719-sensitized solar cells show

2.4 and 6.1% energy conversion efficiency, respectively. The results clearly indicate that the effective binding of the dye to the TiO_2 surface is critical for achieving high efficiency in dye-sensitized solar cells. Reducing the steric hindrance by removing one or two neighbouring phenyl groups might produce dyes with better photovoltaic performance.

Experimental Section

All solvents were treated by standard methods prior to use. Reagent-grade benzaldehyde, 4-methylbenzaldehyde and acetylacetone were obtained commercially and used without further purification. Pyrrole was distilled twice prior to use. Other chemicals were analytical-grade and used as received. The N719 dye was obtained from Solaronix. The FTO glass with a sheet resistance of 8 Ω/cm^2 from Hartfort Glass (USA) was used for cell fabrication. Elemental compositions were determined by using a commercial CHN analyser. The scanning electron microscopy (SEM) images were taken with a Hitachi S3400 microscope. The FTIR spectra were recorded with a Nicolet 6700 spectrometer in ATR mode.

Synthesis of Porphyrins: 5,10,15,20-Tetraphenylporphyrin (H_2TPP) and the 5-(*p*-carboxyphenyl)-10,15,20-tris(4-methylphenyl)porphyrin-zinc complex (ZnTTP-COOH) were prepared according to literature methods.[29]

2-(1-Acetyl-2-oxopropyl)-5,10,15,20-tetraphenylporphyrinatocopper-(II) (CuTPP-AOP): $Cu(NO_3)_2{\cdot}3H_2O$ (0.28 g) and acetic anhydride (18 mL) were added to a solution of CuTPP (0.25 g) in $CHCl_3$ (375 mL). The mixture was magnetically stirred for 48 h at room temperature. The mixture was then washed with water. Then the organic solvent was reduced to around 5 mL, the mixture was loaded on to a silica gel column and eluted with chloroform. The second band, 2-nitro-5,10,15,20-tetraphenylporphyrinatocopper(II) (CuTPP-NO_2), was collected and recrystallized from $CHCl_3$/CH_3OH; yield 0.21 g. The dry CuTPP-NO_2 (0.17 g) was dissolved in DMSO (10 mL). Acetylacetone (257 μL) and anhydrous K_2CO_3 (0.25 g) were added to this solution. The mixture was heated at 50 °C for 1 h and then chloroform (50 mL) and water (20 mL) were added. The organic phase was washed with water several times. After removing all the solvent, the crude product was loaded on to a column of silica gel and eluted with chloroform for purification. The second band was collected. The final product was recrystallized from $CHCl_3$/CH_3OH (5:100, v/v); yield 0.14 g, 78%. $C_{49}H_{34}CuN_4O_2$ (774.38): calcd. C 76.00, H 4.43, N 7.24; found C 75.73, H 4.17, N 7.20. UV/Vis (CH_2Cl_2, 25 °C): λ [log(ε/M^{-1} cm^{-1})] = 417 [5.61], 541 [4.36] nm. MS: calcd. for $C_{49}H_{35}CuN_4O_2$ 774.2; found 774.2. FTIR: $\tilde{\nu}$ = 3051 (w), 3018 (w), 1596 (s) cm^{-1}.

2-(1-Acetyl-2-oxopropyl)-5,10,15,20-tetraphenylporphyrin (H_2TPP-AOP): CuTPP-AOP (0.28 g) was dissolved in CH_2Cl_2 (20 mL) and concentrated H_2SO_4 (5 mL) was added. The resulting mixture was stirred at room temperature for 0.5 h. Then water was added very slowly under vigorous stirring of the reaction mixture. After washing the mixture with water several times, the organic solvent was reduced to around 5 mL with a rotary evaporator and was loaded on to a silica gel column for purification. Chloroform was used to elute the column. The second band was collected. The product was obtained after recrystallization from $CHCl_3$/CH_3OH (5:100, v/v); yield 0.21 g, 84%. $C_{49}H_{36}N_4O_2$ (712.8): C 82.56, H 5.09, N 7.86; found C 82.10, H 4.43, N 7.74. UV/Vis ($CHCl_3$, 25 °C): λ [log(ε/M^{-1} cm^{-1})] = 420 [5.52], 517 [4.29], 551 [3.97], 592 [3.91], 649 [3.82] nm. MS: calcd. for $C_{49}H_{37}N_4O_2$ 713.3; found 713.3. FTIR: $\tilde{\nu}$ = 3051 (w), 3021 (w), 1594 (s) cm^{-1}.

2-(1-Acetyl-2-oxopropyl)-5,10,15,20-tetraphenylporphyrinatozinc(II) (ZnTPP-AOP): H_2TPP-AOP (0.11 g) was dissolved in $CHCl_3$/CH_3OH (1:1, v/v, 25 mL) and excess zinc acetate (0.5 g) was added. The mixture was stirred at room temperature overnight and the organic solvent was removed. The solid was dissolved in a small amount of chloroform and loaded onto a column of silica gel and eluted with chloroform. The main band was collected. The final product was obtained after recrystallization from $CHCl_3$/CH_3OH (5:100, v/v); yield 0.10 g, 83%. $C_{49}H_{34}N_4O_2Zn{\cdot}CH_3OH$: calcd. C 74.30, H 4.74, N 6.93; found C 74.56, H 4.63, N 6.86. UV/Vis ($CHCl_3$, 25 °C): λ [log(ε/M^{-1} cm^{-1})] = 421 [5.68], 549 [4.35] nm. MS: calcd. for $C_{49}H_{35}N_4O_2Zn$ 775.2; found 775.2. FTIR: $\tilde{\nu}$ = 2957 (w), 2927 (w), 1594 (s) cm^{-1}.

X-ray Crystallographic Analysis: Single crystals of ZnTPP-AOP, CuTPP-AOP and H_2TPP-AOP were obtained by slow evaporation of solvent of the complexes in 1:1 (v/v) mixtures of methanol and dichloromethane at room temperature for 2 weeks. The crystals were mounted on glass fibres for data collection. Diffraction measurements were made with a CCD-based commercial X-ray diffractometer using Mo-K_α radiation (λ = 0.71073 Å). The frames were collected at 125 K with a scan width of 0.3° in ω and integrated with the Bruker SAINT software package[30] using a narrow-frame integration algorithm. The unit cell was determined and refined by least-squares methods upon the refinement of *XYZ* centroids of reflections above 20σ(*I*). The data were corrected for absorption by using the SADABS program.[31] The structures were refined on F^2 by using the Bruker SHELXTM (version 5.1) software package.[30]

Crystal Data for ZnTPP-AOP: $C_{49.35}H_{35.39}N_4O_3Zn$, M_r = 797.77, monoclinic, space group = *C*2/*c*, *a* = 41.352(4), *b* = 10.4384(10), *c* = 22.390(2) Å, β = 119.6230(10)°, *V* = 8401.4(14) Å^3, *Z* = 8, $\rho_{calcd.}$ = 1.254 Mg/m^3, μ(Mo-K_α) = 0.630 mm^{-1}, *F*(000) = 3288, *T* = 125(2) K. 40076 reflections were measured, of which 7708 were unique (R_{int} = 0.0571). Final *R*1 = 0.0506 and *wR*2 = 0.1278 values were obtained for 6192 observed reflections with $I > 2\sigma(I)$, 555 parameters and GOF = 1.102.

Crystal data for CuTPP-AOP: $C_{50}H_{35}N_4O_2Cl_2Cu$, M_r = 858.26, triclinic, space group = $P\bar{1}$, *a* = 8.771(2), *b* = 15.038(4), *c* = 16.556(4) Å, α = 114.571(3), β = 94.977(3), γ = 99.032(3)°, *V* = 1933.0(8) Å^3, *Z* = 2, $\rho_{calcd.}$ = 1.475 Mg/m^3, μ(Mo-K_α) = 0.753 mm^{-1}, *F*(000) = 884, *T* = 125(2) K. 18655 reflections were measured, of which 7007 were unique (R_{int} = 0.0541). Final *R*1 = 0.0685 and *wR*2 = 0.2410 values were obtained for 4727 observed reflections with $I > 2\sigma(I)$, 532 parameters and GOF = 1.032.

Crystal data for H_2TPP-AOP: $C_{49}H_{35}N_4O_2$, M_r = 709.76, monoclinic, space group = $P2_1/c$, *a* = 15.103(4), *b* = 10.535(3), *c* = 23.665(7) Å, β = 100.823(18)°, *V* = 3698.5(18) Å^3, *Z* = 4, $\rho_{calcd.}$ = 1.275 Mg/m^3, μ(Mo-K_α) = 0.079 mm^{-1}, *F*(000) = 1484, *T* = 125(2) K. 6826 reflections were measured, of which 6342 were unique (R_{int} = 0.0000). Final *R*1 = 0.1227 and *wR*2 = 0.3715 values were obtained for 2973 observed reflections with $I > 2\sigma(I)$, 497 parameters and GOF = 1.169. Several attempts were carried out to grow high quality crystals of H_2TPP-AOP for X-ray diffraction analysis, but they were not successful.

CCDC-78491 (for ZnTPP-AOP), -78492 (for CuTPP-AOP) and -78493 (for H_2TPP-AOP) contain the supplementary crystallographic data for this paper. These data can be obtained free of charge from The Cambridge Crystallographic Data Centre via www.ccdc.cam.ac.uk/data_request/cif.

Fabrication of DSCs: Free-standing TiO_2 nanotube membranes were prepared as described previously.[28] The FTO glass was first

cleaned successively with toluene, acetone, 2-propanol and deionized water. Then TiO_2 nanoparticles with diameters of around 5 nm prepared by a microwave-assisted sol–gel process was spin-coated on the FTO glass as a compact layer. The film was sintered at 450 °C for 30 min. Then commercial TiO_2 nanoparticle (NP) paste (diameter 9 nm) was screen-printed on to the top of the compact layer. The free-standing TiO_2 NT membrane with a length of around 22 μm was put on to the top of the TiO_2 NP layer. After air-drying for about 0.5 h, a small piece of Parafilm® was placed on top of the film and around 100 g of metal was put on top. The film was kept at –20 °C for 12 h and then air-dried, sintered at 450 °C for 0.5 h in oxygen and cooled to room temperature slowly. The resulting film was dipped into a 2 mM $TiCl_4$ aqueous solution for 1 h and sintered again at 450 °C for 0.5 h. The films were then immersed in 2 mM methanolic solution of the dye for 12 h. The counter-electrode was prepared by sputtering a 10-nm-thick layer of Pt on to the FTO glass. Two electrodes were assembled in a Grätzel-type cell using Surlyn as sealant. The electrolyte solution for porphyrins was 0.10 M LiI, 0.60 M *tert*-butylmethylimidazolium iodide, 0.05 M I_2 and 0.05 M 4-*tert*-butylpyridine in acetonitrile. The electrolyte for N719 was 0.10 M LiI, 0.60 M *tert*-butylmethylimidazolium iodide, 0.05 M I_2 and 0.05 M 4-*tert*-butylpyridine in acetonitrile/valeronitrile (1:1, v/v).

Photocurrent–Voltage Measurements: Photoelectrochemical data were measured using a 450 W xenon light source. The light intensity at the surface of the cell was calibrated to 100 mW/cm^2, equivalent to one sun at air mass 1.5G conditions. The applied potential and cell current were measured by using an Agilent 4155C semiconductor parameter analyser. The efficiency (η) and fill factor (FF) were calculated from η (%) = $100P_{max}/(P_{in}A)$ and FF = $P_{max}/(I_{SC}V_{OC})$, in which P_{max} is the maximum output power of cells (mW), P_{in} is the power density of the light source (mW/cm^2), I_{SC} is the short-circuit current (mA), V_{OC} is the open-circuit voltage (V) and A is the active area (0.16 cm^2) of the cell.

Photophysical Measurements: Absorption spectra were recorded with an HP Agilent 8543 UV/Vis spectrophotometer in CH_2Cl_2 at room temperature. The steady-state fluorescence spectra were obtained with a fluorimeter (FS920, Edinburg Instrument, Inc., UK) with a Xenon arc lamp as the light source. The decay curves of fluorescence were measured with a fluorimeter by using a time-correlated single-photon-counting technique (LifeSpec II, Edinburg Instrument, Inc.). A diode laser (EPL 375, Edinburgh Instrument, Inc., UK) with a wavelength of 375 nm was used as the light source. The pulse repetition frequency was 20 MHz. The lifetimes were determined by exponential fitting of deconvoluted decay curves. Quantum yields were determined according to the literature method by using ZnTPP as the reference standard (Φ = 0.033 in air-equilibrated toluene).[32] Equation (1) was used to calculate the quantum yields in which n_s and n_r are the refractive indices of the solvents of the sample and reference, G_s and G_r are the gradients of the plots of integrated fluorescence intensity versus absorbance for the samples and reference at different concentrations.

$$\phi_s = \phi_r \times \left(\frac{G_s}{G_r}\right) \times \left(\frac{n_s}{n_r}\right)^2 \quad (1)$$

Theoretical Calculations: Theoretical calculations were performed at the density functional theory level. The single-crystal structures were used as frameworks for the construction of initial input structures for the calculations. Geometry optimizations and electronic structure calculations were performed by using the B3LYP functional and the 6-31G(D) basis set in acetonitrile solution by using the conductor-like polarizable continuum model (CPCM) solvation model, as implemented in the Gaussian 09 program package.[33] Acetonitrile was used to mimic the solvents in electrolyte. Molecular orbitals were visualized by GaussView 3.0 software.[33] The method has been widely used for geometry optimizations and electronic calculations of porphyrin derivatives due to its accuracy,[4,5,6,34,35] which was further validated by the very similar bond angles and lengths in the optimized structures of MTPP-AOP (M = $2H^+$, Zn^{2+}, Cu^{2+}) and single-crystal structures.

Supporting Information (see footnote on the first page of this article): ORTEP diagram of H_2TPP-AOP, fluorescence spectra of ZnTPP-AOP and H_2TPP-AOP, and packing diagrams of the three porphyrins.

Acknowledgments

This paper is based on work supported by the National Science Foundation/EPSCoR (grant number 0903804), the State of South Dakota, the Ph. D. program of the Department of Electrical Engineering of the South Dakota State University, the Northern Plain Undergraduate Research Center, and the South Dakota State University Research and Scholar Fund (334578)

[1] M. Grätzel, *Acc. Chem. Res.* **2009**, *42*, 1788–1798.
[2] A. Hagfeldt, G. Boschloo, L. Sun, L. Kloo, H. Pettersson, *Chem. Rev.* **2010**, *110*, 6595–6663.
[3] N. K. S. Davis, A. L. Thompson, H. L. Anderson, *Org. Lett.* **2010**, *12*, 2124–2127.
[4] H. Imahori, Y. Matsubara, H. Iijima, T. Umeyama, Y. Matano, S. Ito, M. Niemi, N. V. Tkachenko, H. Lemmetyinen, *J. Phys. Chem. C* **2010**, *114*, 10656–10665.
[5] C.-F. Lo, S.-J. Hsu, C.-L. Wang, Y.-H. Cheng, H.-P. Lu, E. W.-G. Diau, C.-Y. Lin, *J. Phys. Chem. C* **2010**, *114*, 12018–12023.
[6] A. Kira, Y. Matsubara, H. Iijima, T. Umeyama, Y. Matano, S. Ito, M. Niemi, N. V. Tkachenko, H. Lemmetyinen, H. Imahori, *J. Phys. Chem. C* **2010**, *114*, 11293–11304.
[7] W. W. H. Wong, T. Khoury, D. Vak, C. Yan, D. J. Jones, M. J. Crossley, A. B. Holmes, *J. Mater. Chem.* **2010**, *20*, 7005–7014.
[8] N. R. de Tacconi, W. Chanmanee, K. Rajeshwar, J. Rochford, E. Galoppini, *J. Phys. Chem. C* **2009**, *113*, 2996–3006.
[9] C.-Y. Lin, C.-F. Lo, L. Luo, H.-P. Lu, C.-S. Hung, E. W.-G. Diau, *J. Phys. Chem. C* **2009**, *113*, 755–764.
[10] Y. Liu, N. Xiang, X. Feng, P. Shen, W. Zhou, C. Weng, B. Zhao, S. Tan, *Chem. Commun.* **2009**, 2499–2501.
[11] H. Imahori, S. Hayashi, H. Hayashi, A. Oguro, S. Eu, T. Umeyama, Y. Matano, *J. Phys. Chem. C* **2009**, *113*, 18406–18413.
[12] L. Cheng-Wei, L. Hsueh-Pei, L. Chi-Ming, H. Yi-Lin, L. You-Ren, Y. Wei-Nan, L. Yen-Chun, L. You-Shiang, D. E. Wei-Guang, Y. Chen-Yu, *Chem. Eur. J.* **2009**, *15*, 1403–1412.
[13] H.-P. Lu, C.-Y. Tsai, W.-N. Yen, C.-P. Hsieh, C.-W. Lee, C.-Y. Yeh, E. W.-G. Diau, *J. Phys. Chem. C* **2009**, *113*, 20990–20997.
[14] S. Eu, S. Hayashi, T. Umeyama, A. Oguro, M. Kawasaki, N. Kadota, Y. Matano, H. Imahori, *J. Phys. Chem. C* **2007**, *111*, 3528–3537.
[15] A. J. Mozer, P. Wagner, D. L. Officer, G. G. Wallace, W. M. Campbell, M. Miyashita, K. Sunahara, S. Mori, *Chem. Commun.* **2008**, 4741–4743.
[16] W. M. Campbell, K. W. Jolley, P. Wagner, K. Wagner, P. J. Walsh, K. C. Gordon, L. Schmidt-Mende, M. K. Nazeeruddin, Q. Wang, M. Grätzel, D. L. Officer, *J. Phys. Chem. C* **2007**, *111*, 11760–11762.
[17] L. Giribabu, C. V. Kumar, P. Y. Reddy, *J. Porphyrins Phthalocyanines* **2006**, *10*, 1007–1016.
[18] H. Imahori, T. Umeyama, S. Ito, *Acc. Chem. Res.* **2009**, *42*, 1809–1818.
[19] S. Eu, S. Hayashi, T. Umeyama, Y. Matano, Y. Araki, H. Imahori, *J. Phys. Chem. C* **2008**, *112*, 4396–4405.

[20] C.-Y. Lin, Y.-C. Wang, S.-J. Hsu, C.-F. Lo, E. W.-G. Diau, *J. Phys. Chem. C* **2009**, *113*, 755–764.
[21] T. Bessho, S. Zakeeruddin, C. Y. Yeh, E. G. Diau, M. Grätzel, *Angew. Chem. Int. Ed.* **2010**, *49*, 6646–6649.
[22] Raed Rahal, S. Daniele, L. G. Hubert-Pfalzgraf, V. Guyot-Ferréol, J.-F. Tranchant, *Eur. J. Inorg. Chem.* **2008**, 980–987.
[23] M. Grätzel, *J. Photochem. Photobiol. C: Photochem. Rev.* **2003**, *4*, 145–153.
[24] S. Yoriya, M. Paulose, O. K. Varghese, G. K. Mor, C. A. Grimes, *J. Phys. Chem. C* **2007**, *111*, 13770–13776.
[25] G. K. Mor, K. Shankar, M. Paulose, O. K. Varghese, C. A. Grimes, *Nano Lett.* **2006**, *6*, 215–218.
[26] L. Luo, C.-J. Lin, C.-S. Hung, C.-F. Lo, C.-Y. Lin, E. W.-G. Diau, *Phys. Chem. Chem. Phys.* **2010**, *12*, 12973–12977.
[27] J. R. Jennings, F. Li, Q. Wang, *J. Phys. Chem. C* **2010**, *114*, 14665–14674.
[28] M. Dubey, H. He, *Proceedings of 34th IEEE Photovoltaic Specialist Conference*, Philadelphia, PA, **2009**.
[29] A. D. Adler, F. R. Longo, J. D. Finarelli, J. Goldmacher, J. Assour, L. Korsakoff, *J. Org. Chem.* **1967**, *32*, 476–476.
[30] G. M. Sheldrick, *SHELXTLTM*, reference manual, version 5.1, Madison, WI, **1997**.
[31] G. M. Sheldrick, *SADABS, Empirical Absorption Correction Program*, University of Göttingen, Göttingen, Germany, **1997**.
[32] R. Katoh, A. Furube, T. Yoshihara, K. Hara, G. Fujihashi, S. Takano, S. Murata, H. Arakawa, M. Tachiya, *J. Phys. Chem. B* **2004**, *108*, 4818–4822.
[33] M. J. Frisch, G. W. Trucks, H. B. Schlegel, G. E. Scuseria, M. A. Robb, J. R. Cheeseman, G. Scalmani, V. Barone, B. Mennucci, G. A. Petersson, H. Nakatsuji, M. Caricato, X. Li, H. P. Hratchian, A. F. Izmaylov, J. Bloino, G. Zheng, J. L. Sonnenberg, M. Hada, M. Ehara, K. Toyota, R. Fukuda, J. Hasegawa, M. Ishida, T. Nakajima, Y. Honda, O. Kitao, H. Nakai, T. Vreven, J. A. Montgomery Jr., J. E. Peralta, F. Ogliaro, M. Bearpark, J. J. Heyd, E. Brothers, K. N. Kudin, V. N. Staroverov, R. Kobayashi, J. Normand, K. Raghavachari, A. Rendell, J. C. Burant, S. S. Iyengar, J. Tomasi, M. Cossi, N. Rega, J. M. Millam, M. Klene, J. E. Knox, J. B. Cross, V. Bakken, C. Adamo, J. Jaramillo, R. Gomperts, R. E. Stratmann, O. Yazyev, A. J. Austin, R. Cammi, C. Pomelli, J. W. Ochterski, R. L. Martin, K. Morokuma, V. G. Zakrzewski, G. A. Voth, P. Salvador, J. J. Dannenberg, S. Dapprich, A. D. Daniels, Ö. Farkas, J. B. Foresman, J. V. Ortiz, J. Cioslowski, D. J. Fox, *Gaussian 09, Revision A.1*, Gaussian, Inc., Wallingford, CT, **2009**.
[34] M. P. Balanay, D. H. Kim, *Phys. Chem. Chem. Phys.* **2008**, *10*, 5121–5127.
[35] C.-Y. Lin, Y.-C. Wang, S.-J. Shu, C.-F. Lo, E. W.-G. Diau, *J. Phys. Chem. C* **2010**, *114*, 687–693.

Received: February 22, 2011
Published Online: July 28, 2011

